A Novel Microwave Tomography System Based on the Scattering Probe Technique

Majid Ostadrahimi, *Student Member, IEEE*, Puyan Mojabi, *Member, IEEE*, Sima Noghanian, *Senior Member, IEEE*, Lotfollah Shafai, *Life Fellow, IEEE*, Stephen Pistorius, *Senior Member, IEEE*, and Joe LoVetri, *Senior Member, IEEE*

***Abstract*—In this paper, we introduce a novel microwave tomography system, which utilizes 24 double-layered Vivaldi antennas, each of which is equipped with a diode-loaded printed-wire probe. By biasing the probe's diodes, the impedance of the probe is modified, allowing an indirect measurement of the electric field at the probe's locations. Each printed-wire probe is loaded with five equally spaced p-i-n diodes, in series. We show that electric field data collected in this way within the proposed tomography system can be used to reconstruct the dielectric properties of an object of interest. Reconstructions for various objects are shown. Although the results are still preliminary, sufficient experimentation has been done to delineate the advantages of such an indirect method of collecting scattered-field data for tomographic imaging purposes.**

***Index Terms*—Microwave tomography (MWT), modulated scatterer technique (MST), near-field measurement, p-i-n diode.**

I. Introduction

MICROWAVE TOMOGRAPHY (MWT) is an imaging modality that uses electromagnetic radiation to reconstruct a quantitative image of the dielectric properties of an object of interest (OI). In MWT, fields are measured at some probing sites outside the OI. An inverse scattering algorithm is then utilized to reconstruct the shape, location, and dielectric properties of the OI from these measured fields. Current indications of algorithms and experimental systems are that MWT can be useful for nondestructive testing and biomedical applications, e.g., see [1]–[10] and references therein.

There are two common approaches for data acquisition in current MWT systems, both of which measure the received voltage at the port of one or more of the receiving antennas in the system. In the first approach, the measured voltage is used to infer the electromagnetic field impinging directly on the receiving antenna. This requires that some sort of antenna factor be, implicitly or explicitly, part of the calibration procedure. It also requires that the receiving antenna be located at the points where the electromagnetic field needs to be measured. This has been accomplished by either repositioning the receiving antenna or using an array of co-resident receiving antennas. Various types of antennas have been used in conjunction with this approach, e.g., monopoles [6], open-ended waveguides [8], and double-layered Vivaldi antennas (DLVAs) [11].

Within the framework of this direct approach, we have developed an "air-based" MWT system that utilizes 24 DLVAs located around the periphery of a Plexiglas chamber of diameter 45.5 cm [11]. The DLVAs are connected to a vector network analyzer (VNA) through a 24×2 radio-frequency (RF) switch/multiplexer. Each DLVA, individually, illuminates the OI, whereas the remaining antennas collect the scattered field, thus providing $24 \times 23 = 552$ data points at each frequency. Successful image reconstructions have been demonstrated using this MWT system [12], [13].

The second approach uses the measured voltage at the receiving antenna to infer the electromagnetic field impinging on a probe positioned at some distance from the receiving antenna. In an early use of this approach [14], an array of dipole probes was positioned in front of a single receiving antenna, which, in this case, is a horn antenna. In the state-of-the-art use of this indirect method for MWT, two horn antennas having a 30-cm square aperture are located on either side of a water tank and used as the sole transmitter (Tx) and the sole receiver (Rx) [15]. The distance between the two horn apertures is 20 cm, and a 32×32 array of dipole probes is positioned in front of the Rx antenna. Each probe is loaded using a p-i-n diode and is sequentially modulated at a low frequency, producing a scattered field at the Rx antenna. This probe-scattered field is proportional to the original field at the probe location [16], [17]. As in the direct approach, a calibration procedure is required to infer the field at each probe [15]. The method is well known as the modulated scatterer technique (MST). Different forms of probe modulation can be used. Electronic [18], optical [19], and mechanical [20] modulation techniques have been reported in the literature.

This indirect approach of measurement offers several advantages over the direct approach. First, increasing the number of observation points can be easily accommodated by simply adding more probes, whereas, in the direct approach, this

Manuscript received November 25, 2010; revised May 17, 2011; accepted June 17, 2011. Date of publication August 18, 2011; date of current version January 5, 2012. This work was supported in part by the Natural Sciences and Engineering Research Council of Canada, by the CancerCare MB, by the Canadian Foundation for Innovation, by the University of North Dakota, and by the University of Manitoba Graduate Fellowship program. The Associate Editor coordinating the review process for this paper was Dr. Sergey Kharkovsky.

M. Ostadrahimi, P. Mojabi, L. Shafai, and J. LoVetri are with the Department of Electrical and Computer Engineering, University of Manitoba, Winnipeg, MB R3T 5V6, Canada (e-mail: morahimi@ee.umanitoba.ca; joe_lovetri@umanitoba.ca).

S. Noghanian was with the Department of Electrical and Computer Engineering, University of Manitoba, Winnipeg, MB R3T 5V6, Canada. She is now with the Department of Electrical Engineering, University of North Dakota, Grand Forks, ND 58202-8382 USA.

S. Pistorius is with CancerCare Manitoba, Winnipeg, MB R3E 0V9, Canada, and also with the Department of Physics and Astronomy, University of Manitoba, Winnipeg, MB R3T 5V6, Canada.

Color versions of one or more of the figures in this paper are available online at http://ieeexplore.ieee.org.

Digital Object Identifier 10.1109/TIM.2011.2161931

requires either adding more antennas to the co-resident antenna arrays or accurately repositioning the Rx antenna or array to more physical locations. Physically repositioning is difficult and time consuming to perform accurately. Not only is increasing the size of the co-resident array expensive because of the need for RF switches but adding array elements also increases mutual coupling, which must then be taken into account in the imaging algorithm and calibration procedure. Adding more probes is usually a simple matter, and the probe modulation is achieved using inexpensive low-frequency switching circuitry. In addition, the mutual coupling between probes is much less than that between Rx antennas, particularly because only one probe is "activated" at a time. (The remaining probes are kept "open" and therefore have minimal interaction with the RF field.)

On the other hand, because the probe-scattered field, upon which the indirect approach relies, is relatively small, custom coherent detectors are typically used for such systems. This requires measurement averaging over a large number of modulation cycles to improve the signal-to-noise ratio (SNR). In [15], the data are averaged over 500 measurements. Due to the small probe-scattered field, the probes must be placed close to the Rx antenna, limiting the number of locations surrounding the OI at which the probes can be placed.

To the best of our knowledge, only bistatic MST has been reported for imaging applications (e.g., see [14], [15], and [21]). In the bistatic implementation, there is only one Rx antenna and one Tx antenna incorporated with an array of probes in front of the Rx. In this feasibility study, we utilize a combination of the direct and indirect methods for the MWT application. The purpose is to quantitatively investigate the performance of the proposed technique, where, instead of using a single Tx and an array of probes in front of a single Rx antenna, we equip each DLVA of our air-based system with a scattering probe in its vicinity (for a total of 24 probes). These probes surround the OI with equal angular spacing of 15°. Each probe is simply a printed dipole whose impedance is changed electronically by biasing the five equally separated p-i-n diodes located along its length. The routing of the biasing wires is chosen via accurate field simulations of the DLVA/probe setup to minimize any field perturbations. It is shown that increasing the number of p-i-n diodes decreases the interaction of the probe and receiver antenna, but interaction between each DLVA and its probe still exists.

Measurements to collect field data within the MWT chamber are performed by successively activating and deactivating each scattering probe. While the impedance of the active probe is changed, the remaining probes are kept "open." The "closing" and "opening" of the active probe generate a differential signal at each of the DLVAs. This differential signal is strongest at the DLVA nearest to the active probe, which we refer to as the "collector." A data acquisition program connects the nearest collector to the VNA and records the differential signal, which is proportional to the field at the active probe's location. In Section II, an overview of the complete system is provided, and details of the scattering-probe design are given in Section III. The measurement and calibration methodology is described in Section IV.

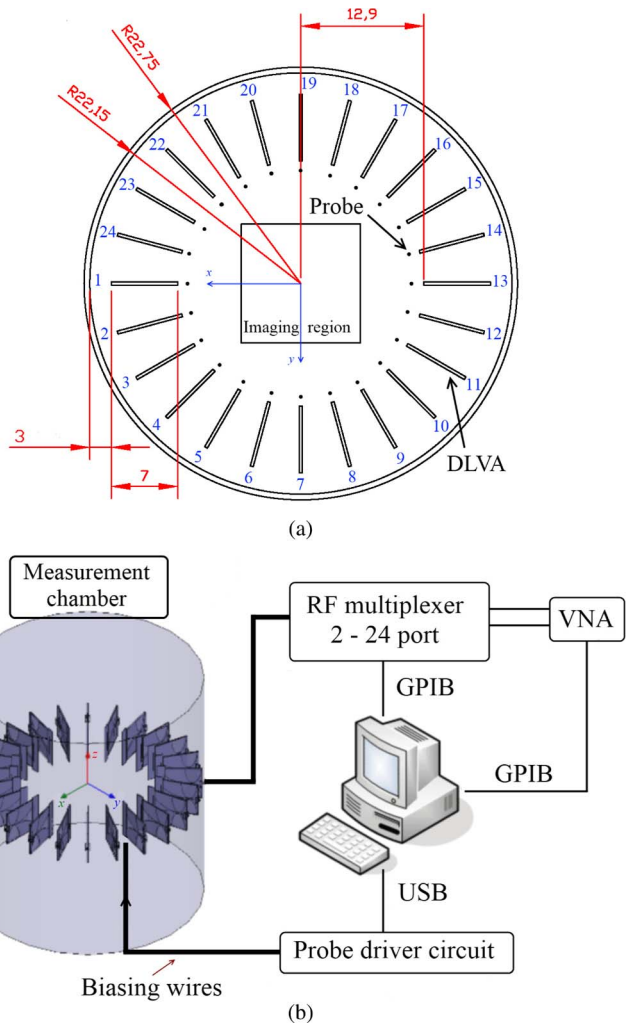

Fig. 1. (a) Top view of the measurement chamber. (Dimensions are in centimeters.) (b) Block diagram of the MWT system.

Different OIs, including a complicated target (which we refer to as the e-phantom), two nylon rods, and a combination of polyvinyl chloride (PVC) with a nylon rod are used to test the proposed system. Images of the OIs are successfully reconstructed using the multiplicative regularized Gauss–Newton inversion (MR-GNI) algorithm [4]. An overview of the algorithm is given in Section V. Imaging results are provided in Section VI, followed by a discussion in Section VII. Conclusions are drawn in Section VIII.

II. MWT System Description

The measurement system consists of four subsystems, which will be described now. The dimensions of the chamber and a block diagram of the system are provided in Fig. 1. A photo of the system during the measurement of the e-phantom object is shown in Fig. 2.

A. Measurement Chamber and Antennas

Twenty-four DLVAs are mounted on a Plexiglas cylinder that is 50.8 cm tall with equal angular spacing of 15°. The

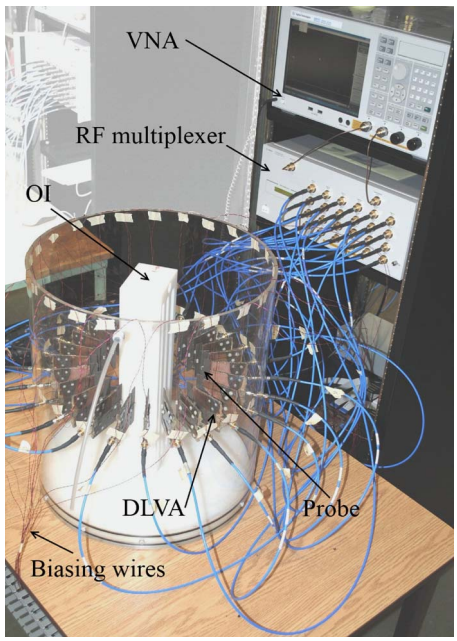

Fig. 2. Measurement system during collection of the e-phantom data set.

DLVA is designed for an ultrawideband frequency range of 3.1–10.6 GHz. This antenna consists of two layers held together by seven nylon screws. Compared to a single-layer Vivaldi antenna, the double-layer version presents at least a 10-dB improvement in the cross-polarization performance [22]. This is an advantage of our imaging algorithm, which assumes a 2-D transverse magnetic field distribution or simply just assumes that only E_z exists. The overall size of each DLVA is 7 cm $\times$ 7 cm. The only difference with respect to the previous direct experimental system reported in [12] is that each DLVA is now equipped with a scattering probe, which is located at a distance of 3 mm in front of it. The imaging region is a centered square, as depicted in Fig. 1(a).

B. RF Multiplexer and VNA

A 2–24-port RF electromechanical multiplexer (Agilent 85070A) is used to switch to a chosen active Tx or Rx antenna. The isolation between ports is 95 dB. The multiplexer is connected to two ports of an Agilent 5071C VNA. The multiplexer and the VNA are both controlled by the data acquisition program via the controller computer unit. Their connection is established through a general-purpose interface bus (GPIB).

C. Probe Driver Circuit

To switch the probes to close/open states, which correspond to forward/reversed biases of p-i-n diodes, respectively, a 24-Darlington-pair-transistor array is used. The transistors are connected to a 24-port Universal Serial Bus (USB) input/output card, which is controlled by the data acquisition program. Using high-precision resistors, the forward bias current for all 24 probes are adjusted with less than 1% tolerance.

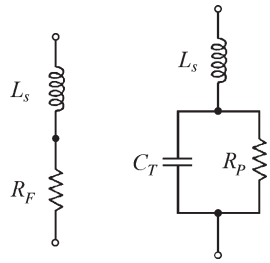

Fig. 3. Equivalent circuit for the p-i-n diode. (Left, close) Forward bias. (Right, open) Reversed bias.

D. Controller Computer

A data acquisition program controls all the instruments. A computer is directly connected to the probe driver circuit module via a USB connection. The multiplexer and the VNA are connected through a GPIB-Ethernet hub. For collecting each data set, a Tx antenna is first chosen by switching it to one of the VNA ports. For each Tx antenna, the other 23 Rx antennas are switched sequentially to the second port of the VNA, resulting in $24 \times 23 = 552$ measurements at each frequency. Each collector (Rx DLVA) collects two measurements, i.e., one with the nearest probe closed and one with the nearest probe opened. During these two measurements, the remaining probes are kept open. (Thus, they have minimal effects on the measurements.) The total data acquisition time for each frequency is less than 4 min. Currently, the acquisition time is limited to the mechanical RF-switch settling time.

III. Probe Design

Each scattering probe consists of a printed dipole on a small piece of substrate of the same type as is used for the DLVA (Arlon DiClad 527 with a thickness 62.5 mil and a relative permittivity of 2.5). The probe length and width are 42.8 and 0.5 mm, respectively. This corresponds to a half-wavelength at 3.505 GHz.

To open and close each probe, five p-i-n diodes are placed in series at equally spaced positions on the probe. Each probe substrate is attached to a DLVA using two small nylon screws (2 mm). The distance between the probe and the DLVA is 3 mm, with the probe copolarized with the DLVA.

A. p-i-n Diode Characterization

The p-i-n diode equivalent circuit model for the forward and reversed bias cases is shown in Fig. 3. Currently, we use BAR64-02V p-i-n diodes from Infineon.

To model the presence of the p-i-n diodes, one requires a simulation method that combines a full-wave solver and a circuit simulator. Developing such a combined simulation tool enables us to calculate the equivalent circuit of the p-i-n diode using an optimization method. The S_{21} coefficient of the diode on a 50-Ω transmission line is provided by the factory. We used the Ansoft Nexxim circuit solver to simulate the circuit part (Fig. 3) and the Ansoft HFSS finite-element method (FEM) solver to simulate a 50-Ω microstrip transmission line. Using

TABLE I
DIODE CALCULATED EQUIVALENT CIRCUIT PARAMETERS

Symbol	Value
R_F	0.5 Ω
L_s	0.6 nH
R_p	4.0 KΩ
C_T	0.0718 pF

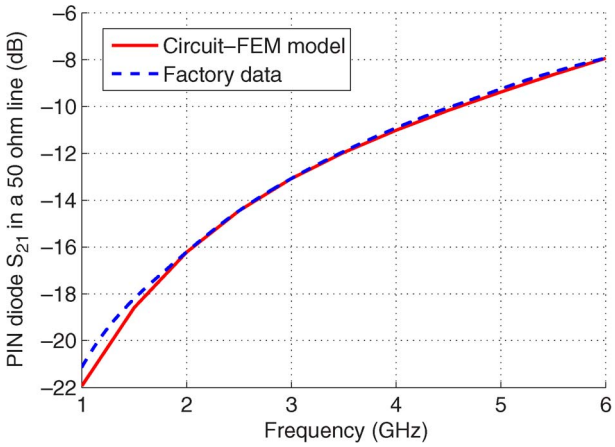

Fig. 4. p-i-n diode reverse bias insertion loss from factory data and optimized circuit model.

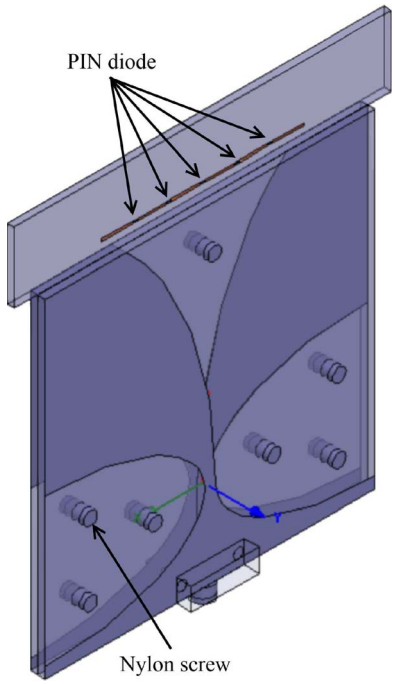

Fig. 5. Simulating the probe–DLVA response, using the Circuit-FEM solver.

the combined simulation, which we refer to as the circuit-FEM solver, and the quasi-Newton optimization technique, we calculated the equivalent circuit components. The optimized values are listed in Table I.

A comparison of the calculated S_{21} and the factory data is shown in Fig. 4. There is a good agreement between the results.

B. Probe Configuration

Using the circuit-FEM solver, the reflection coefficient of the DLVA was simulated in two cases: 1) when the probe is closed (forward-biased diodes) and 2) when it is opened (reversed-biased diodes). The simulation geometry is shown in Fig. 5. We also studied the effect of using different numbers of p-i-n diodes. For this study, three different simulations were performed: 1) a probe with a single diode located at its center, 2) a probe with three diodes in series, and 3) a probe with five diodes in series, located equally spaced along the probe.

In the closed case, the changes in reflection coefficient for the three cases are negligible (less than 0.2 dB). This is due to the small insertion loss of the p-i-n diodes.

In the open case, increasing the number of p-i-n diodes resulted in a performance that is more similar to that of the DLVA alone. These results are compared in Fig. 6. According to this comparison, we concluded that increasing the number of p-i-n diodes decreases the interference of the generated fields of the DLVA in Tx mode; thus, we chose the configuration with five p-i-n diodes.

C. Designing the Biasing Route

The bias current is a dc current and does not interfere with the RF signal; however, the biasing circuitry and wires must not itself significantly perturb the fields. Thus, we used the FEM method (Ansoft HFSS) to numerically model the field distribution in the vicinity of the DLVAs, at various frequencies, to determine the optimal routing of the biasing circuitry and wires. Fig. 7 shows the distribution of fields at 3.5 and 5.0 GHz. As shown in the figure, the field intensity is stronger at the corners of the DLVA, and they are in different directions. However, the central region shows a smaller variation of fields, and the field vectors are, mostly, along the z-axis. Based on these observations and considering the probe length, we chose a bias line parallel to the x-axis between the nylon screws. Rosin is used as the adhesive to secure the biasing wires to the DLVA. A picture of the probe mounted in front of the

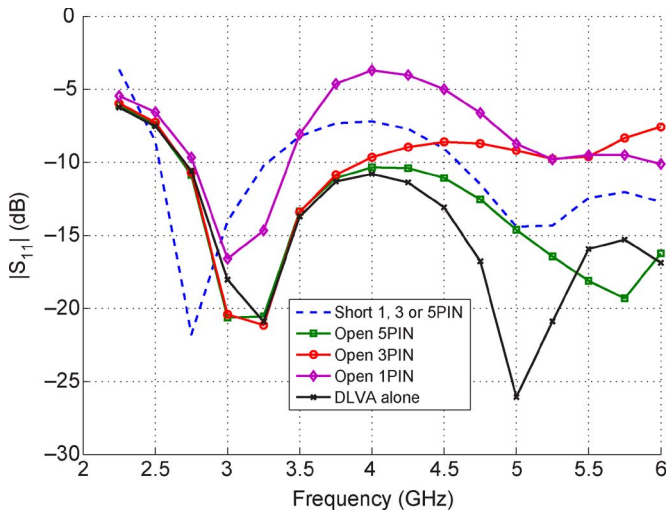

Fig. 6. Simulated reflection coefficient of a DVLA near a probe loaded with one, three, and five p-i-n diodes, in series.

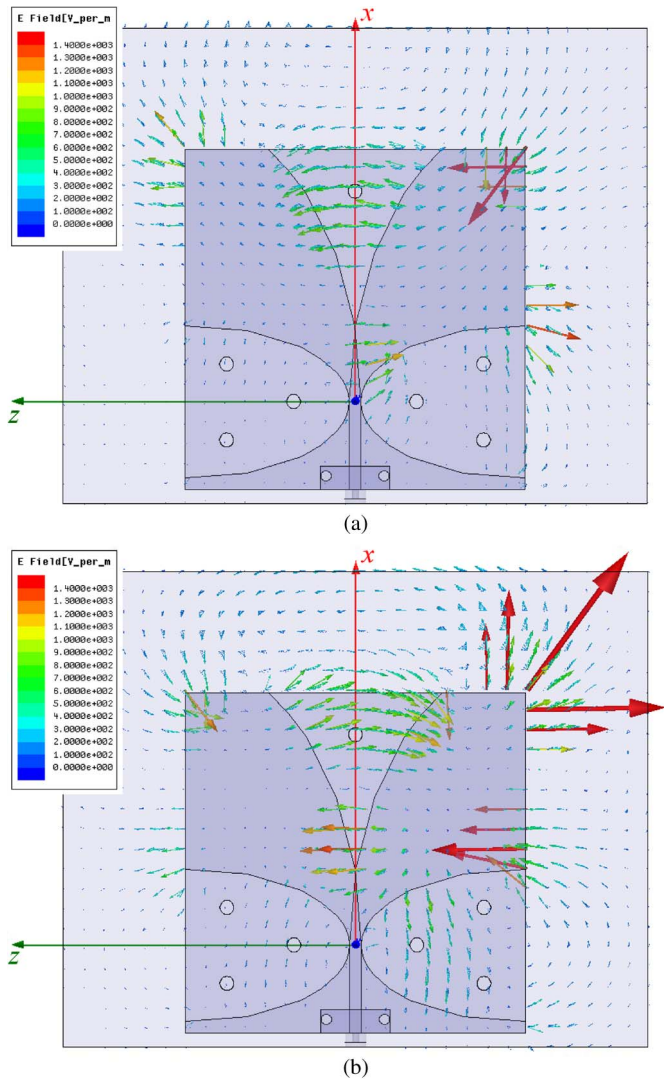

Fig. 7. Field distribution of a single DLVA alone. (a) 3.5 GHz. (b) 5.0 GHz.

DLVA is shown in Fig. 8. Two surface-mounted "termination" resistors are added to either side of the probe. These resistors "terminate" the RF current at both ends of the probe. Using this configuration, our measurements showed that the change in the reflection coefficient, due to the presence of the biasing wires, is less than 2 dB within the frequency range of 1–6 GHz. We also tried some other routes, e.g., from the corners of the DLVA. Measurement results show that the biasing wires along other routes interfere with the DLVA by more than 5 dB.

IV. Measurement Method

For the imaging algorithm, the field scattered by the OI is required at each probe location. Each measurement at a probe's location is performed by changing the impedance of that probe. The probe whose impedance is changing is called the active probe. When a probe is active, the remaining probes are kept "open," so they remain "invisible" to electromagnetic fields. The impedance change produces change in the measured voltage at the nearest collector (Rx DLVA), which is proportional

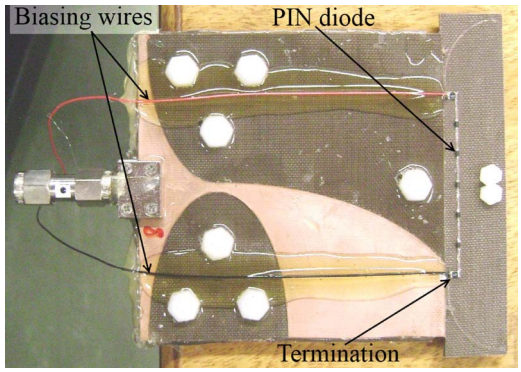

Fig. 8. Fabricated DLVA and a probe.

to the field at the active probe's location. This is what we call the MST procedure.

To measure the scattered field, the total field (i.e., with the OI present in the measurement chamber) and the incident field (i.e., with the OI absent in the measurement chamber) are collected using the MST procedure. Thus, with one Tx DLVA transmitting, the impedance of each active probe is changed by opening and closing its diodes while keeping all of the remaining probes open. The Tx DLVA is connected to one port of the VNA, whereas the nearest collector to the active probe (Rx DLVA) is connected to the second port of the VNA. The impedance change in the active probe in front of the collector generates a change in VNA transmission coefficient S_{21} between the Tx DLVA and the collector. Denoting the measured scattering parameters in the two cases of closing and opening the active probe as $S_{21}^{\rm sc}$ and $S_{21}^{\rm oc}$, respectively, the difference between these two measurements is defined as $\delta S_{21} = S_{21}^{\rm sc} - S_{21}^{\rm oc}$.

Once the incident (no OI present) and total (OI present) fields are measured by this technique, the scattered field generated by the OI is calculated by subtracting the total and incident fields: $E_z^{\rm sct} = E_z^{\rm tot} - E_z^{\rm inc}$. The total and incident fields are thus proportional to $\delta S_{21}^{\rm tot}$ and $\delta S_{21}^{\rm inc}$, respectively; thus, the scattered field due to the OI satisfies $E_z^{\rm sct} \propto \delta S_{21}^{\rm sct}$, where $\delta S_{21}^{\rm sct} = \delta S_{21}^{\rm tot} - \delta S_{21}^{\rm inc}$.

In our experimental system, the thin probes are parallel to the z direction, and they interact mainly with E_z. A current is generated on the probe that is proportional to the E_z field component. The MST procedure is based on the assumption that the differential δS_{21} is proportional to the field at the probe's location. The theoretical background of this statement is discussed in detail in [16]. However, we attempted to validate this assumption for a simpler case of one DLVA acting as both Tx and Rx while a probe is located in front of it. Using Ansoft HFSS, we performed two simulations: 1) computing the E_z fields of a DLVA at different locations, without the presence of any probe, and 2) computing the field, using the MST procedure with a probe parallel to the z-axis. In this simulation, we computed the DLVA differential reflection coefficient δS_{11} for every location of the probe. The results of the two simulations agreed with each other.

Note that the MST procedure is effective in removing some sources of experimental error, e.g., errors due to cable movement, as well as the noise generated in the multiplexer unit and the network analyzer. The time interval between the two

MST measurements is very short, and we assume that the cables remain stationary and unchanged during this interval.

A. Calibration

Our 2-D imaging algorithm models neither the antennas nor the entire 3-D measurement system, and this results in modeling error. Moreover, the field excitation is implemented by a line source placed at the Tx antenna's location, instead of a DLVA in the presence of co-resident DLVAs. This is another source of modeling error. Finally, in addition to modeling error, measurement errors must also be taken into account. To reduce the effects of these errors, the data collected by the probes should be calibrated. To calibrate the data, we used a perfect electric conductor (PEC) cylinder with 3.5-in diameter as the reference object. The scattered field produced by this reference object is collected using the MST procedure, as discussed in the previous section. For any active transmitter, an individual calibration factor is defined for each probe. That is, $23 \times 24 = 552$ calibration factors are defined for each frequency of operation. For an active transmitter, the calibration factor at each probing site $\mathcal{C}_{\mathcal{F}}$ is the ratio of the analytical scattered field by the PEC cylinder to the measured scattered field at that probe's location, i.e.,

$$\mathcal{C}_{\mathcal{F}} = E_z^{\text{sct,analytic}} / \delta S_{21}^{\text{sct,PEC}} \tag{1}$$

where $E_z^{\text{sct,analytic}}$ is the analytical solution of the scattered field by the PEC cylinder in the vicinity of a line source, and $\delta S_{21}^{\text{sct,PEC}}$ is the measured data, which is proportional to the actual scattered field in the presence of the PEC cylinder. A comparison of $E_z^{\text{sct,analytic}}$ and $\delta S_{21}^{\text{sct,PEC}}$ at 4.5 GHz is shown in Fig. 9.

Five hundred fifty-two calibration factors are stored in the column vector $\underline{\mathcal{C}_{\mathcal{F}}} \in \mathbb{C}^{552}$. The measured data $\delta S_{21}^{\text{sct}}$, which represents the scattered field due to the OI at a given frequency, is also stored in the column vector $\underline{\delta S_{21}^{\text{sct}}} \in \mathbb{C}^{552}$. The calibrated measured scattered-field data, which are denoted by $\underline{E}^{\text{meas}}$, are then obtained as $\underline{E}^{\text{meas}} = \underline{\mathcal{C}_{\mathcal{F}}} \odot \underline{\delta S_{21}^{\text{sct}}}$, where $\odot$ denoted the Hadamard product between two vectors of the same size. This calibrated measured scattered field is then used by the inversion algorithm to reconstruct the relative complex permittivity of the OI.

B. Probe Sensitivity to the Incident Power

To measure the field at the probe location, the changes of the probe impedance should be detectable by the VNA. We refer to this parameter as the sensitivity of the probe to the input power to the chamber. We measured the incident field at each of the 24 DLVA locations, whereas the VNA output power was set to -5 dBm. For each measurement, the impedance of the nearest probe to the receiver DLVA was changed to record δS_{21}. Choosing the two antennas with the greatest separation, i.e., choosing antennas "1" and "13" [see Fig. 1(a)] as the transmitter and the receiver, respectively, the lowest δS_{21} was observed to be greater than -50 dB. This measurement is shown in Fig. 10 over the bandwidth of interest. For the same

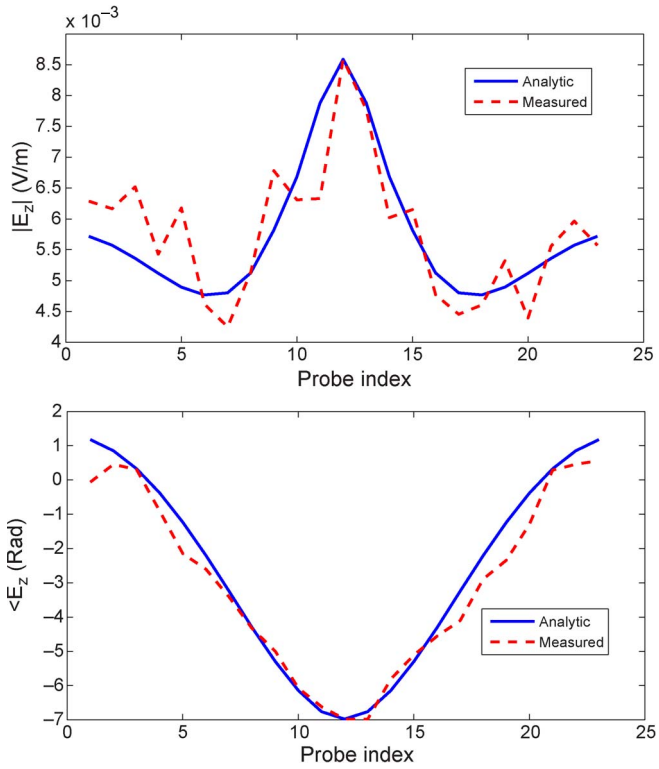

Fig. 9. Comparison of the scattered field by the reference PEC cylinder from the analytic solution and the scaled MST measurement at 4.5 GHz.

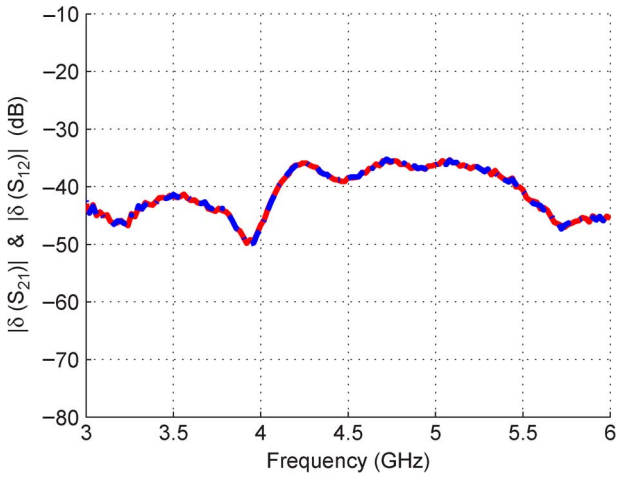

Fig. 10. δS_{21} for Tx:1 and Rx:13. Incident power is -5 dBm.

Tx/Rx pair, which produced the lowest δS_{21}, we decreased the VNA output power from -5 dBm, in steps of 5 dB, down to the -35 dBm. At an output power level of -35 dBm, the measurements reached the noise floor; thus, we conclude that the probes are sensitive to an input power of as low as -30 dBm. For this measurement, we did not use any averaging technique to reduce the noise floor. In addition to δS_{21} measurement, we measured the change in reflection coefficient of the receiver antenna, which is an indication of probe interaction with the receiver. We collected the change in reflection coefficient δS_{22} of one of the DLVAs in the measurement chamber when the nearest probe impedance was changed. As shown in Fig. 11, the reflection coefficient ranges from -15 to -23 dB, at the frequency range of

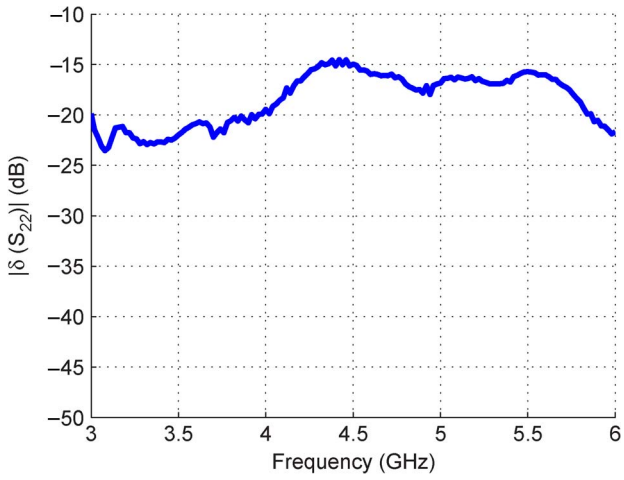

Fig. 11. δS_{22} measurement in the tomography system, as an indication of probe-DLVA interaction.

3–6 GHz. Fig. 6 illustrates the simulated "open" and "short" cases of the idealized configuration shown in Fig. 5. In simulation, we did not consider the presence of the co-resident DLVAs or the biasing circuitry. Therefore, Figs. 6 and 11 are presented separately.

We also investigated averaging the measured data to improve the SNR. In this technique, the signal is averaged over a number of repeated measurements to obtain a higher SNR, e.g., 500-time averaging has improved the SNR on the order of 25 dB in the MWT system reported in [15]. We collected several data sets using the proposed measurement system. For each data set, we collected the field by applying an averaging of 1, 5, 10, 100, and 1000 times. The change in MST signal in all cases was less than 0.2 dB, whereas the VNA output power was set to -5 dBm. There were negligible changes observed in the data sets or in the images resulting from these data sets. We concluded that averaging is therefore not required, allowing faster one-shot data acquisition.

V. Inversion Algorithm

We denote the imaging and measurement domains by $\mathcal{D}$ and $\mathcal{S}$, respectively, both of which are in $\mathbb{R}^2$. In addition, let $\mathbf{r}$ denote the position vector in $\mathbb{R}^2$. The imaging domain is immersed in a known background having a relative complex permittivity of ϵ_b, which contains a nonmagnetic OI with an unknown relative complex permittivity $\epsilon_r(\mathbf{r})$. (In our case, the background medium is air.) Assuming $e^{j\omega t}$ time dependence, the relative complex permittivity of the OI can be written as $\epsilon_r(\mathbf{r}) = \epsilon_r'(\mathbf{r}) - j\epsilon''(\mathbf{r})$. The contrast function, which is defined as

$$\chi \triangleq \frac{\epsilon_r(\mathbf{r}) - \epsilon_b}{\epsilon_b} \tag{2}$$

is to be found using the measured scattered field on $\mathcal{S}$. Once χ is found, the relative complex permittivity of the OI can be easily recovered. In our implementation, the contrast function is discretized into N square pulses; thus, the contrast function is represented by the complex vector $\underline{\chi} \in \mathbb{C}^N$. Assuming the 2-D transverse magnetic illumination, the electric field can be represented by a single component perpendicular to the measurement and imaging domains. Denoting $\underline{E}^{\text{meas}}$ as the calibrated measured scattered field on $\mathcal{S}$ and $\underline{E}^{\text{sct}}(\underline{\chi})$ as the simulated scattered field on $\mathcal{S}$ due to the predicted contrast $\underline{\chi}$, the MWT problem may be formulated as the minimization over $\underline{\chi}$ of the following data misfit cost-functional:

$$\mathcal{F}^{\text{LS}}(\underline{\chi}) = \frac{1}{\|\underline{E}^{\text{meas}}\|_{\mathcal{S}}^2} \left\|\underline{E}^{\text{sct}}(\underline{\chi}) - \underline{E}^{\text{meas}}\right\|_{\mathcal{S}}^2 \tag{3}$$

where $\|\cdot\|_{\mathcal{S}}$ denotes the L_2-norm on $\mathcal{S}$. It is well known that the data misfit cost-functional $\mathcal{F}^{\text{LS}}(\underline{\chi})$ is nonlinear and ill-posed. There are different methods, such as the modified gradient method [3], [23] and the Gauss-Newton method [4], [24], to treat the nonlinearity of this cost-functional. The ill-posedness of the problem is treated by employing an appropriate regularization technique [25]. In this paper, we utilize the weighted L_2-norm total variation multiplicative regularizer within the framework of the Gauss–Newton method. The details of this method, which we refer to as the MR-GNI method, can be found in [4] and [26].

VI. Imaging Results

Using the proposed experimental system and the MR-GNI algorithm, we image the relative complex permittivity of three different OIs. These tests include the following: 1) resolution test; 2) complexity test; and 3) combination test.

The objects are positioned at the center of the measurement chamber. The MST data set is collected at the frequencies of 3–5 GHz with a step of 0.5 GHz. For all cases, images of the OIs were successfully reconstructed. In addition to the single-frequency inversion, multiple-frequency inversion was also utilized to reconstruct the OIs. In multiple-frequency inversion, we assumed that the dielectric properties of the OIs are invariant at all frequencies.

For the resolution test, the results of the single- and multiple-frequency inversions are presented. For the complexity and the combination test, the best single-frequency image (at 4.5 GHz) and the multiple-frequency image are presented. We speculate that the image at 4.5 GHz is the best result due to minimum mismatch between the simulated and measured data, corresponding to the reference object utilized for calibration at this frequency.

A. Resolution Test

For this test, we used two nylon rods whose separation is 4 mm. This OI is shown in Fig. 12(a). The dimensions are listed in Table II. The relative permittivity of the nylon is 3.03-j0.03 ($\chi = 2.03 - \text{j}0.03$) [27]. The imaging results of the single-frequency inversion and the multiple-frequency inversion are shown in Fig. 13 where the separation changes from $\lambda/25$ at 3 GHz to $\lambda/15$ at 5 GHz. For this test, the imaging region is a 12-cm square and is discretized to 60×60 pixels. The real part of the nylons' reconstructed relative complex permittivity is close to its expected value (particularly at 4.5 GHz). We also note that the nylon rods are almost lossless; thus, the inversion algorithm is not capable of reconstructing the imaginary part of

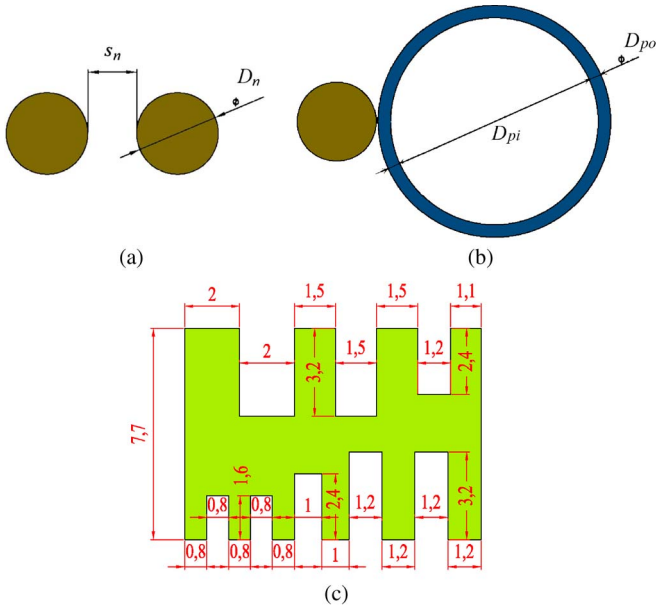

Fig. 12. OIs for image reconstruction. (a) Resolution test. (b) Combination test. (c) Complexity test (e-phantom, dimensions in centimeters).

TABLE II
DIMENSIONS OF OIs (IN CENTIMETERS) (FIG. 12)

Symbol	D_n	s_n	D_{po}	D_{pi}
Dimension	3.8	0.4	13.0	10.2

the relative complex permittivity of the nylon rods due to the limited SNR and dynamic range of the system.

B. Combination Test

Fig. 12(b) illustrates a combination of a PVC cylinder adjacent to a nylon rod, which is used for the combination test. The dimensions are listed in Table II. The PVC relative permittivity is $\epsilon_r \approx 2.5 - j0.01$ at 4.5 GHz [13]. The imaging results are shown in Fig. 14. For this test, the imaging region is a square measuring 17 $\times$ 17 cm and is discretized to 70 $\times$ 70 pixels. The multiple-frequency reconstruction of this target is more accurate, compared to its single-frequency reconstruction.

C. Complexity Test

In this experiment, we used a complex e-phantom object, as shown in Fig. 12(c). This object was first introduced in [28]. The e-phantom is made of UltraHigh Molecular Weight polyethylene (UHMW) with a relative permittivity of $\epsilon_r = 2.3$. The loss of UHMW is negligible [13]. The dimensions are shown in Table II and Fig. 12(c). Imaging results of single (4.5 GHz) and multiple frequencies are shown in Fig. 15. For this test, the imaging region is a 13-cm square and is discretized to 80 $\times$ 80 pixels. For multiple-frequency inversion, the data set at 3–5 GHz with a frequency step of 0.5 GHz is used. Similar to the results presented in [13] and [28], features with a minimum size of 1 cm and above are resolved, whereas the two concave features of 0.8 cm are not resolved.

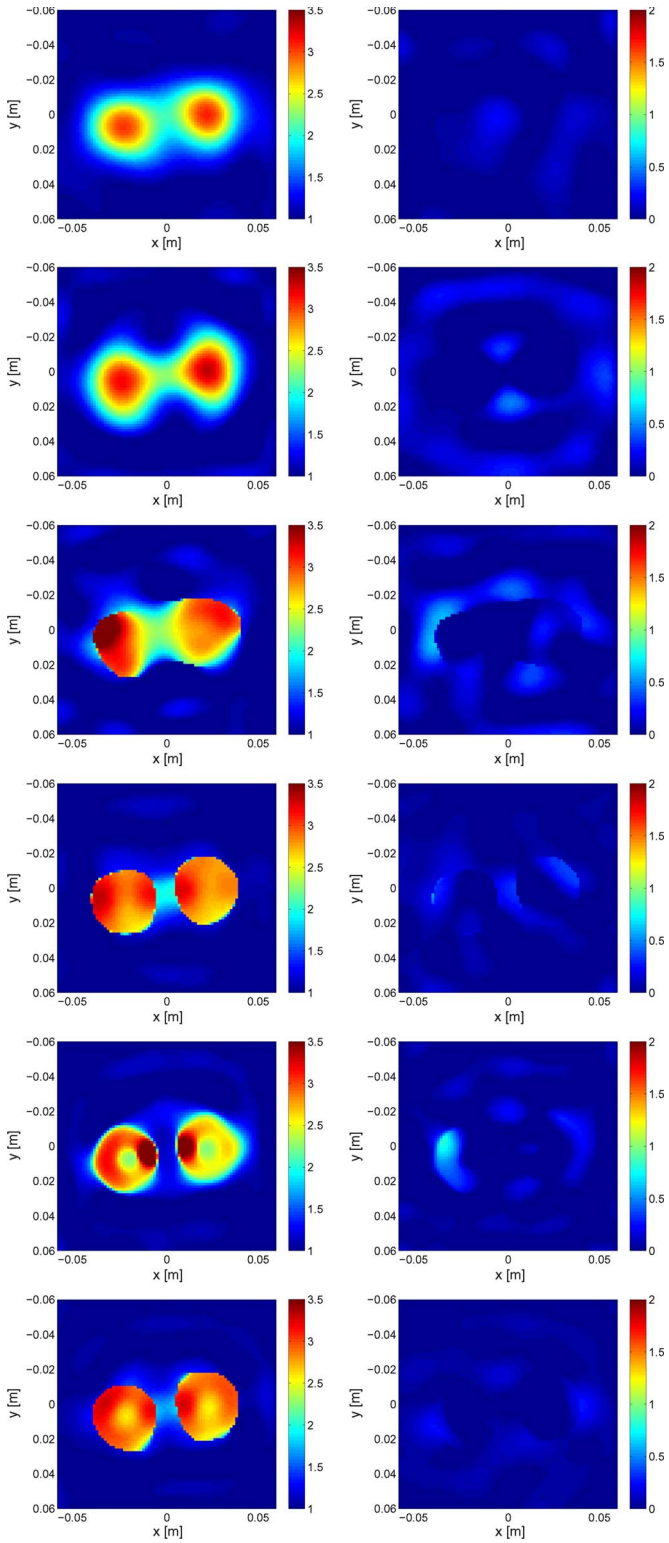

Fig. 13. Reconstructed (left) real and (right) negative of imaginary parts of the relative complex permittivity of the resolution test object with a separation of 4 mm at (first row) 3.0 GHz, (second row) 3.5 GHz, (third row) 4.0 GHz, (fourth row) 4.5 GHz, (fifth row) 5.0 GHz, and (last row) multiple-frequency inversion, respectively.

D. Inversion Results of Synthetic Data

We created a synthetic data set with 3% additive white noise (according to the formula given in [29]) of the e-phantom

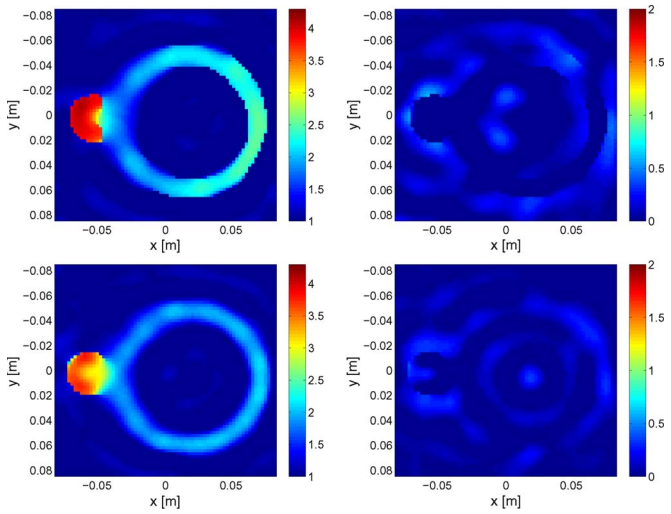

Fig. 14. Reconstructed (left) real and (right) negative of imaginary parts of the relative complex permittivity of the combination test object at (first row) 4.5 GHz and (second row) multiple-frequency inversion, respectively.

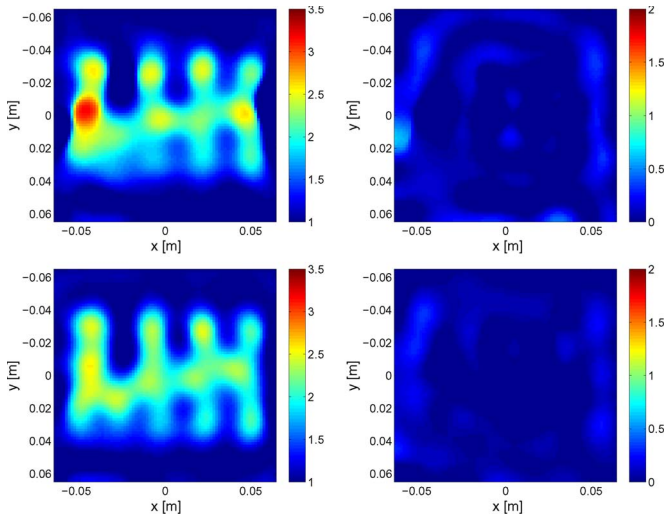

Fig. 15. Reconstructed (left) real and (right) negative of imaginary parts of the relative permittivity of the complexity test object at (first row) 4.5 GHz and (second row) multiple-frequency inversion, respectively.

(complexity test). This synthetic data set is created with the method of moments, using 24 line sources, positioned at the same location as the probes in the measurement system. Imaging results from this synthetic data set are shown in Fig. 16. The results of synthetic data inversion, as shown in Fig. 16, can be compared with those of the measured data, as shown in Fig. 15. Overall, the reconstruction results are similar; however, the quantitative accuracy of the reconstructed image from the synthetic data is slightly higher than that from the measured data.

VII. Discussion

Configuration of the "air-based" MWT system introduces two major sources of measurement error, i.e., instrumentation error and polarization error. The polarization error is due to the antennas not being able to differentiate between different polarizations of field within the chamber, whereas instrumentation error is introduced by the measurement system being used.

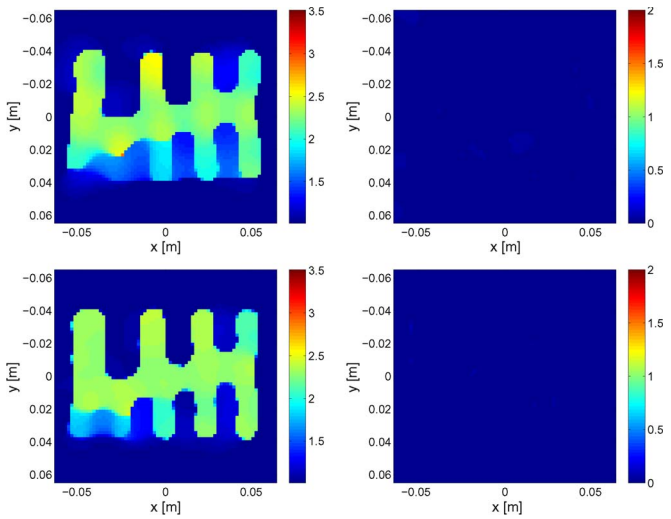

Fig. 16. Synthetic data reconstructed and (left) real and (right) negative of imaginary parts of the relative permittivity of the complexity test object at (first row) 4.5 GHz and (second row) multiple-frequency inversion, respectively.

In our experimental system, the antennas remain stationary; thus, the polarization error remains constant throughout the measurements. Instrumentation error is a function of several factors, which may be time varying, i.e., room temperature; imperfection in the cables being used, which may vary due to cable movement; and VNA calibration errors between measurements.

In the direct measurement system (no probe), the time difference between different data collections introduces a time-varying instrumentation error that is mostly due to the cables. This is because the cables are not necessarily stationary, and their stress and bending may change in time. Reducing this error requires repeating the incident-field and the calibration measurements for each data collection. As mentioned earlier, the incident-field and calibration measurements are required by the inversion algorithm.

In the system being proposed, every field measurement is performed twice by repeating the S_{21} measurement, when the probes are open and when they are closed. The two measurements are performed within a short period of each other, during which we assume that the cables remain unchanged. This applies to the incident field, total field, and PEC cylinder calibration measurements. Due to the collection of differential signals at each measurement, the cable errors almost vanish. Having said that, there is no need to repeat the incident field or the PEC measurement, and this is one of the advantages of this system.

Another disadvantage of the direct measurement system is the limitation of the number of possible measurement locations. In such a system, an increase in measurement locations requires the presence of more co-resident antennas. This increases mutual coupling, particularly in a free-space environment such as that considered herein, where there is no loss to reduce the coupling. Furthermore, adding more antennas to the co-resident array requires the use of more expensive RF switches. In these systems, there is a tradeoff between mutual coupling and the number of field sampling points using antennas. Increasing the number of co-resident antennas increases the mutual coupling. On the other hand, using fewer antennas reduces the number of

field sampling points. One of the advantages of the proposed system is its potential for decreasing the number of antennas and increasing the number of probes, thereby increasing the number of field-sampling points. (We are currently investigating the extent to which we can take advantage of such a procedure.) Using numerical experiments, we had studied the number of antennas for our "direct" systems. The results depended on the object type being imaged. In most cases, 24 antennas were the best choice between increasing the number of co-resident antennas and minimizing the mutual coupling. We did not study this issue experimentally.

In the proposed MST technique, the simple scattering probes are the primary measurement devices that surround the OI and are impedance modulated successively to collect the field. The DLVAs produce the initial field and are only a secondary receiving device. Due to the use of differential measurement, the instrumentation error is reduced. In addition, since the cable error is removed, it is possible to rotate parts of the measurement system to collect more data. Moreover, we do not need to repeat the incident and calibration measurement, even if there is a long time gap between measurements. As long as the position of the antennas and probes inside the chamber remains unchanged, the incident and calibration measurements are valid. This is an advantage for possibly future clinical systems. For the image reconstructions presented here, the data sets were collected over an interval of several days without repeating the incident or the calibration measurement. The cables were moved during this period.

For future study, because this system has the ability to measure (infer) any field at a scattering-probe site, it can also be used with an "incident-field-type" calibration, as opposed to the scattered-field calibration described herein. There may be advantages to such a calibration technique. In terms of increasing the number of probing locations, because the proposed technique is less expensive to implement, we will investigate the use of more scattering probes per antenna.

Compared to direct and indirect methods, we benefit from the advantages of both methods. Data measurement is fast and is collected in a single-shot measurement. We did not see any change in the reconstructed images by averaging the data being collected. We used the MR-GNI algorithm to successfully reconstruct images of different objects.

VIII. Conclusion

A novel measurement system based on the MST technique has been introduced. In this system, measurements are performed in the near-field region using a primary array of scattering probes in front of a secondary array of receiving antennas. A direct measurement system with 24 DLVA had been developed in our laboratory. To test the feasibility of the proposed system, a minimum number of probes (equal to number of DLVAs) has been incorporated into the system.

To implement the MST, each scattering probe has been opened and closed by biasing the p-i-n diodes positioned in series along the probe. A careful analysis of the system has been performed for choosing the optimum biasing route. The sensitivity of the probe has also been measured by decreasing the VNA output power. Using the MR-GNI inversion algorithm, successful images of different objects have been reconstructed.

The proposed system features a number of advantages: incident-field and calibration measurements have been performed only once. The system reduces instrumentation error, as well as measurement errors due to the cables. It can also measure incident and total fields directly. Moreover, it is possible to rotate the system and increase the number of probes without a need for RF switches.

Acknowledgment

The authors would like to thank the anonymous reviewers for their thorough and useful comments.

References

[1] S. Semenov, "Microwave tomography: Review of the progress towards clinical applications," *Philos. Trans. A Math. Phys. Eng. Sci.*, vol. 367, no. 1900, pp. 3021–3042, Aug. 2009.

[2] N. Joachimowicz, C. Pichot, and J. Hugonin, "Inverse scattering: An iterative numerical method for electromagnetic imaging," *IEEE Trans. Antennas Propag.*, vol. 39, no. 12, pp. 1742–1753, Dec. 1991.

[3] A. Abubakar, P. Van den Berg, and J. Mallorqui, "Imaging of biomedical data using a multiplicative regularized contrast source inversion method," *IEEE Trans. Microw. Theory Tech.*, vol. 50, no. 7, pp. 1761–1771, Jul. 2002.

[4] P. Mojabi and J. LoVetri, "Microwave biomedical imaging using the multiplicative regularized Gauss–Newton inversion," *IEEE Antennas Wireless Propag. Lett.*, vol. 8, pp. 645–648, 2009.

[5] T. Rubæk, P. Meaney, P. Meincke, and K. Paulsen, "Nonlinear microwave imaging for breast-cancer screening using Gauss–Newton's method and the cgls inversion algorithm," *IEEE Trans. Antennas Propag.*, vol. 55, no. 8, pp. 2320–2331, Aug. 2007.

[6] P. Meaney, M. Fanning, D. Li, S. Poplack, and K. Paulsen, "A clinical prototype for active microwave imaging of the breast," *IEEE Trans. Microw. Theory Tech.*, vol. 48, no. 11, pp. 1841–1853, Nov. 2000.

[7] R. Halter, T. Zhou, P. Meaney, A. Hartov, J. Barth, Jr., K. Rosenkranz, W. Wells, C. Kogel, A. Borsic, E. Rizzo, and K. D. Paulsen, "The correlation of *in vivo* and *ex vivo* tissue dielectric properties to validate electromagnetic breast imaging: Initial clinical experience," *Physiolog. Meas.*, vol. 30, no. 6, p. S121, Jun. 2009.

[8] S. Semenov, A. Bulyshev, A. Abubakar, V. Posukh, Y. Sizov, A. Souvorov, P. van den Berg, and T. Williams, "Microwave-tomographic imaging of the high dielectric-contrast objects using different image-reconstruction approaches," *IEEE Trans. Microw. Theory Tech.*, vol. 53, no. 7, pp. 2284–2294, Jul. 2005.

[9] J. Geffrin and P. Sabouroux, "Continuing with the Fresnel database: Experimental setup and improvements in 3D scattering measurements," *Inverse Probl.*, vol. 25, no. 2, p. 024 001, Feb. 2009.

[10] T. Rubæk, O. Kim, and P. Meincke, "Computational validation of a 3-D microwave imaging system for breast-cancer screening," *IEEE Trans. Antennas Propag.*, vol. 57, no. 7, pp. 2105–2115, Jul. 2009.

[11] M. Ostadrahimi, S. Noghanian, L. Shafai, A. Zakaria, C. Kaye, and J. LoVetri, "Investigating a double layer vivaldi antenna design for fixed array field measurement," *Int. J. Ultra Wideband Commun. Syst.*, vol. 1, no. 4, pp. 282–290, 2010.

[12] C. Gilmore, P. Mojabi, A. Zakaria, M. Ostadrahimi, C. Kaye, S. Noghanian, L. Shafai, S. Pistorius, and J. LoVetri, "A wideband microwave tomography system with a novel frequency selection procedure," *IEEE Trans. Biomed. Eng.*, vol. 57, no. 4, pp. 894–904, Apr. 2010.

[13] C. Gilmore, P. Mojabi, A. Zakaria, S. Pistorius, and J. LoVetri, "On super-resolution with an experimental microwave tomography system," *IEEE Antennas Wireless Propag. Lett.*, vol. 9, pp. 393–396, 2010.

[14] J. Bolomey, L. Jofre, and G. Peronnet, "On the possible use of microwave-active imaging for remote thermal sensing," *IEEE Trans. Microw. Theory Tech.*, vol. MTT-31, no. 9, pp. 777–781, Sep. 1983.

[15] T. Henriksson, N. Joachimowicz, C. Conessa, and J. Bolomey, "Quantitative microwave imaging for breast cancer detection using a planar 2.45 GHz system," *IEEE Trans. Instrum. Meas.*, vol. 59, no. 10, pp. 2691–2699, Oct. 2010.

[16] J. Bolomey and F. Gardiol, *Engineering Applications of the Modulated Scatterer Technique*. Norwood, MA: Artech House, 2001.
[17] S. Caorsi, M. Donelli, and M. Pastorino, "A passive antenna system for data acquisition in scattering applications," *IEEE Antennas Wireless Propag. Lett.*, vol. 1, no. 1, pp. 203–206, 2002.
[18] R. Harrington, "Small resonant scatterers and their use for field measurements," *IRE Trans. Microw. Theory Tech.*, vol. 10, no. 3, pp. 165–174, May 1962.
[19] H. Memarzadeh-Tehran, J. Laurin, and R. Kashyap, "Optically modulated probe for precision near-field measurements," *IEEE Trans. Instrum. Meas.*, vol. 59, no. 10, pp. 2755–2762, Oct. 2010.
[20] A. Cullen and J. Parr, "A new perturbation method for measuring microwave fields in free space," *Proc. Inst. Elect. Eng. B—Radio Electron. Eng.*, vol. 102, no. 6, pp. 836–844, Nov. 1955.
[21] M. Ghasr, M. Abou-Khousa, S. Kharkovsky, R. Zoughi, and D. Pommerenke, "A novel 24 GHz one-shot, rapid and portable microwave imaging system," in *Proc. IEEE Instrum. Meas. Tech. Conf.*, 2008, pp. 1798–1802.
[22] M. Ostadrahimi, S. Noghanian, and L. Shafai, "A modified double layer tapered slot antenna with improved cross polarization," in *Proc. ANTEM/URSI 13th Int. Symp. Antenna Tech. Appl. Electromagn.*, 2009, pp. 1–4.
[23] R. Kleinman and P. Van Den Berg, "A modified gradient method for two-dimensional problems in tomography," *J. Comput. Appl. Math.*, vol. 42, no. 1, pp. 17–35, Sep. 1992.
[24] W. Chew and Y. Wang, "Reconstruction of two-dimensional permittivity distribution using the distorted born iterative method," *IEEE Trans. Med. Imag.*, vol. 9, no. 2, pp. 218–225, Jun. 1990.
[25] P. Mojabi and J. LoVetri, "Overview and classification of some regularization techniques for the Gauss–Newton inversion method applied to inverse scattering problems," *IEEE Trans. Antennas Propag.*, vol. 57, no. 9, pp. 2658–2665, Sep. 2009.
[26] A. Abubakar, T. Habashy, V. Druskin, L. Knizhnerman, and D. Alumbaugh, "2.5D forward and inverse modeling for interpreting low-frequency electromagnetic measurements," *Geophysics*, vol. 73, no. 4, pp. F165–F177, Jul. 2008.
[27] R. F. Harrington, *Time-Harmonic Electromagnetic Fields*. New York: IEEE Press, 2001.
[28] S. Semenov, R. Svenson, A. Bulyshev, A. Souvorov, A. Nazarov, Y. Sizov, V. Posukh, A. Pavlovsky, P. Repin, and G. Tatsis, "Spatial resolution of microwave tomography for detection of myocardial ischemia and infarction-experimental study on two-dimensional models," *IEEE Trans. Microw. Theory Tech.*, vol. 48, no. 4, pp. 538–544, Apr. 2000.
[29] A. Abubakar, P. Van Den Berg, and S. Semenov, "A robust iterative method for born inversion," *IEEE Trans. Geosci. Remote Sens.*, vol. 42, no. 2, pp. 342–354, Feb. 2004.

Majid Ostadrahimi (S'09) received the B.Sc. degree in electrical engineering from Sharif University of Technology, Tehran, Iran, in 2003 and the M.Sc. (with distinction) degree in electrical engineering from Iran University of Science and Technology, Tehran, in 2006. He is currently working toward the Ph.D. degree at the Department of Electrical and Computer Engineering, University of Manitoba, Winnipeg, MB, Canada.

His current research interests include near-field measurement and modulated scatterer technique, microwave tomography and inverse problems, and computational electromagnetics.

Mr. Ostadrahimian has been the IEEE Winnipeg Section Treasurer since 2010.

Puyan Mojabi (M'10) received the B.Sc. degree from the University of Tehran, Tehran, Iran, in 2002, the M.Sc. degree from Iran University of Science and Technology, Tehran, in 2004, and the Ph.D. degree from the University of Manitoba, Winnipeg, MB, Canada, in 2010, all in electrical engineering.

He is currently an Assistant Professor with the Department of Electrical and Computer Engineering, University of Manitoba. His current research interests are computational electromagnetics, antenna design, and inverse problems.

Sima Noghanian (M'03–SM'05) received the B.Sc. degree from Sharif University of Technology, Tehran, Iran, in 1992 and the M.Sc. and Ph.D. degrees from the University of Manitoba, Winnipeg, MB, Canada, in 1996 and 2001, respectively, all in electrical engineering.

In 2001, she was with YottaYotta Corporation, Edmonton, AB, Canada. She received a Postdoctoral Fellowship from Natural Sciences and Engineering Research Council of Canada in 2002, which she took at the University of Waterloo, Waterloo, ON, Canada. She was an Assistant Professor with the Department of Electrical Engineering, Sharif University of Technology, during 2002–2003. From 2003 to 2008, she was an Assistant Professor with the Department of Electrical and Computer Engineering, University of Manitoba. Since 2008, she has been an Assistant Professor with the Department of Electrical Engineering, University of North Dakota, Grand Forks. Her research interests include antenna design and modeling, wireless channel modeling, ultrawideband antennas, and microwave imaging.

Dr. Noghanian served as the IEEE Winnipeg Waves Chapter (joint Chapter of Antenna & Propagation, Microwave Theory & Techniques, and Vehicular Technology societies) Chair during 2004–2005.

Lotfollah Shafai (S'67–M'69–SM'75–F'88–LF'07) received the B.Sc. degree from the University of Tehran, Tehran, Iran, in 1963 and the M.Sc. and Ph.D. degrees from the University of Toronto, Toronto, ON, Canada, in 1966 and 1969, all in electrical engineering.

In November 1969, he joined the Department of Electrical and Computer Engineering, University of Manitoba, Winnipeg, MB, Canada, as a Sessional Lecturer. He became an Assistant Professor in 1970, Associate Professor in 1973, and Professor in 1979. Since 1975, he has made special effort to link the university research to the industrial development by assisting industries in the development of new products or establishing new technologies. To enhance the University of Manitoba's contact with the industry, in 1985, he assisted in establishing "The Institute for Technology Development" and was its Director until 1987, when he became the Head of the Department of Electrical Engineering. His assistance to the industry was instrumental in establishing an Industrial Research Chair in Applied Electromagnetics at the University of Manitoba in 1989, which he held until July 1994.

Dr. Shafai was a Fellow of The Royal Society of Canada in 1998, The Canadian Academy of Engineering in 2002, and the Engineering Institute of Canada in 2009. He has been a Distinguished Professor with The University of Manitoba. He holds a Canada Research Chair in Applied Electromagnetics and was the International Chair of Commission B of the International Union of Radio Science (URSI) from 2005 to 2008. He has been a participant in nearly all Antennas and Propagation Symposia and participates in the review committees. He is a member of URSI Commission B and was its Chairman during 1985–1988. In 1986, he established the symposium Antenna Technology and Applied Electromagnetics (ANTEM), which is currently held every two years at the University of Manitoba. In 1978, his contribution to the design of a small ground station for the Hermus satellite was selected as the 3rd Meritorious Industrial Design. He was the recipient of numerous awards, including the Professional Engineers Merit Award in 1984; "The Thinker" Award from Canadian Patents and Development Corporation in 1985; the "Research Awards" from the University of Manitoba in 1983, 1987, and 1989; the Outreach Award in 1987; the Sigma Xi Senior Scientist Award in 1989; the Maxwell Premium Award from IEE (London) in 1990; the Distinguished Achievement Awards from Corporate Higher Education Forum in 1993 and 1994; the Winnipeg RH Institute Foundation Medal for Excellence in Research in 1998; the University of Manitoba Faculty Association Research Award in 1999 and 2000; the IEEE Third Millenium Medal in 2000; an IEEE Canada "Reginald A. Fessenden Medal" for "Outstanding Contributions to Telecommunications and Satellite Communications" and a Natural Sciences and Engineering Research Council (NSERC) Synergy Award for "Development of Advanced Satellite and Wireless Antennas" in 2003; an IEEE Chen-To-Tai Distinguished Educator Award in 2009; and a Killam Prize in Engineering from The Canada Council for the Arts, for his "outstanding Canadian career achievements in engineering, and his work in antenna research," in 2011.

Stephen Pistorius (SM'08) received the B.Sc. degree from the University of Natal, Natal, South Africa, in 1982 and the B.Sc. (Hons.) degree in radiation physics, the M.Sc. degree in medical science, and the Ph.D. degree in physics degree from the University of Stellenbosch, Stellenbosch, South Africa, in 1983, 1984, and 1991, respectively.

He is currently a Full Professor in physics and astronomy and an Associate Professor in radiology with the Department of Physics and Astronomy, University of Manitoba, Winnipeg, MB, Canada, and a Senior Research Scientist with CancerCare Manitoba, Winnipeg. He is the author of more than 100 publications and presentations. His research interests are cancer imaging for both early detection and optimized radiation therapy.

Prof. Pistorius is a certified Medical Physicist, has served as the President of the Canadian Organization of Medical Physics, and is currently the Academic Director of the CAMPEP-accredited Medical Physics graduate program at the University of Manitoba and the Director of Professional Affairs for the Canadian Association of Physicists. He is the recipient of a number of national and international awards.

Joe LoVetri (SM'00) received the B.Sc. (with distinction) and M.Sc. degrees in electrical engineering from the University of Manitoba, Winnipeg, MB, Canada, in 1984 and 1987, respectively, the Ph.D. degree in electrical engineering from the University of Ottawa, Ottawa, ON, Canada, in 1991, and the M.A. degree in philosophy from the University of Manitoba in 2006.

From 1984 to 1986, he was an EMI/EMC Engineer with the Sperry Defence Division, Winnipeg, and from 1986 to 1988, he held the position of TEMPEST Engineer with the Communications Security Establishment, Ottawa, ON, Canada. From 1988 to 1991, he was a Research Officer with the Institute for Information Technology, National Research Council of Canada. His academic career began in 1991 when he joined the Department of Electrical and Computer Engineering, The University of Western Ontario, London, ON, Canada, where he remained until 1999. During 1997–1998, he spent a sabbatical year at the TNO Physics and Electronics Laboratory, The Netherlands, doing research in time-domain computational methods and ground-penetrating RADAR. In 1999, he joined the University of Manitoba, where he is currently a Professor with the Department of Electrical and Computer Engineering. From 2004 to 2009, he was the Associate Dean (Research and Graduate Programs) for the Faculty of Engineering. His research interests include time-domain computational electromagnetics, modeling of electromagnetic compatibility problems, inverse problems, and biomedical imaging.